arXiv:0903.4348v1 [cond-mat.other] 25 Mar 2009

Breathing oscillations and quasi-low-dimensional shell-structures of fermion condensates in super-anisotropic traps

Takushi Nishimura[1,*] and Tomoyuki Maruyama[2,3,4,†]

[1]*Division of Advanced Sciences, Ochadai Academic Production, Ochanomizu University, Otsuka, Bunkyo, Tokyo 112-8610, Japan*

[2]*College of Bioresource Sciences, Nihon University, Fujisawa 252-8510, Japan*

[3]*Advanced Science Research Center, Japan Atomic Energy Research Institute,Tokai 319-1195, Japan*

[4]*Department of Physics, Tokyo Metropolitan University, Hachioji, Tokyo 192-0397, Japan*

Abstract

We theoretically investigate breathing oscillations of fermion condensates in anisotropic harmonic oscillator traps. When anisotropy of the trap is not large, the Fermi gases behave as three-dimensional (3D) gases, and those breathing oscillations are studied in the previous work [1]; when the trap is super-anisotropic, the fermions show quasi-low-dimensional (QLD) properties differently from the 3D gases because of variation of one-particle energy-level densities, which exhibit specific types of shell-structures, *QLD shell-structures*, in super-anisotropic systems. In the present work, we study the effects of the QLD shell-structures on the breathing oscillations of the week-interacting fermion condensates with same number densities. The QLD shell-structures are described in the semi-classical Thomas-Fermi approximation (TFA) extended to the super-anisotropic systems, and the collective frequencies of the breathing oscillations are estimated in the scaling and sum-rule methods with the perturbation theory and extended TFA up to the first order in a coupling constant of inter-atomic interaction. As a result, we reveal that the effects of the QLD shell-structures on the collective frequencies disappear in transverse modes in both of the oblate and prolate deformed traps, and appear only in longitudinal modes with hierarchic structures associated with the trap anisotropy. We also demonstrate time-evolution of the oscillations in the present framework.

PACS numbers: 03.75.Ss,67.85.Lm,37.10.Gh,05.30.Fk

*nishimura.takushi@ocha.ac.jp

†maruyama.tomoyuki@nihon-u.ac.jp

I. INTRODUCTION

Development of the trapping and cooling techniques of atoms yields many and various studies on trapped ultracold atomic gases. One can now study the Bose-Einstein condensates (BECs) [2, 3, 4], the degenerate Fermi gases (or fermion condensates) [5, 6], and mixtures of them [7, 8, 9, 10]. In particular, the two-component Fermi gases are recently well-studied in various interaction regimes: In attraction regime, the Feshbach resonance method realize the atomic pair condensates in the BCS theory and molecular BEC (the BCS-BEC crossover) [11, 12]; in strong repulsion regime, the repulsion induce a phase transition from paramagnetic states to ferromagnetic and phase-separation states [13]. In addition, the quasi-low-dimensional (QLD) atomic gases are also realized in super-anisotropic traps [14, 15, 16, 17, 18, 19, 20, 21, 22], which often show quite different behaviors from the three-dimensional (3D) gases. Those systems offer great infrastructure of fundamental study on quantum many-particle systems.

One of important features in the quantum many-particle systems is the collective excitations, which are often sensitive to interaction and structure of microscopic quantum states, and must reflect the QLD properties. In particular, the breathing oscillations give important diagnostic signals for global properties of the trapped quantum gases in the actual experiments. Those collective excitations are theoretically treated with the time-dependent mean-field theory, which is reduced to the random-phase approximation (RPA) for small amplitude excitations [23, 24, 25]. When the one-particle spectrum is regular and exhibits the collective excitations in the long-wavelength range, one can use simpler methods to calculate the frequencies of the collective oscillations: e.g. the sum-rule method [26] and the scaling method [1, 27, 28, 29].

In Ref. [29], one of the authors and his collaborator study spin excitations on dipole and monopole oscillations in the 3D two-component Fermi gases in the spherical trap using the scaling method. In that work, we discuss the mixing of the in-phase and out-of-phase oscillation modes and show the relations between the oscillation frequencies and the phase of the two-component Fermi gases [13].

In Ref. [1], furthermore, we study the breathing oscillations of the two-component fermion condensates in anisotropic harmonic oscillator traps with various trap frequencies, and demonstrate the mixing behavior of breathing oscillations in the longitudinal and trans-

verse directions. In that work, however, we assume that anisotropy of the traps is not so large, and apply the conventional Thomas-Fermi approximation (TFA) for the 3D gases to predict the collective frequencies of the breathing oscillations in the scaling method. Thus it is needed to improve the approach when we study the collective oscillations in the QLD systems.

In this paper, then, we extend those studies on the breathing oscillations of the 3D gases to the super-anisotropic deformed gases with the QLD properties, which gradually appear as the trap anisotropy increases. The QLD properties should originally be given in the microscopic approach, where the quantum many-body properties can be described with the shell-structures of the one-particle spectrum by using the one-particle picture, so that, in principle, we can consider the QLD properties as exhibition of specific types of shell-structures, *QLD shell-structures*, in the super-anisotropic systems. The precise properties of the QLD shell-structures are studied and discussed in the present work.

The aim of the present work is to reveal the QLD properties on the breathing oscillations of the fermion condensates and describe the crossover behaviors between the 3D and QLD gases. To simplify the subject, we focus on the breathing oscillations of the week-interacting fermions with same number densities, i.e. the in-phase breathing oscillations, and use the perturbation theory and semi-classical TFA to calculate the parameters needed in the scaling and sum-rule methods.

The content of this paper is as follows. In Section II, we give the theoretical framework in this work: theoretical explanations of the trapped Fermi gases and breathing oscillations and formulation of the scaling and sum-rule methods. In Section III, we consider the ground state properties reflecting the QLD shell-structures by developing TFA to the super-anisotropic systems in order to calculate the parameters needed in the scaling and sum-rule methods. In Section IV, we show calculational results of the collective frequencies and demonstrate time-evolution in the present framework. In Section V, we give summary and outlook.

II. THEORETICAL FRAMEWORK

A. Trapped Fermi gases

Let us take two-component gases of fermionic atoms of A_1 and A_2 species with same atomic masses, $m_1 = m_2 \equiv m$, in same trap potentials, $V_1(\boldsymbol{r}) = V_2(\boldsymbol{r}) \equiv V(\boldsymbol{r})$. The Hamiltonian is denoted as

$$H^{(\mathrm{tc})} = \sum_{\alpha=1}^{2} \int d\boldsymbol{r}\ \Psi_\alpha^\dagger(\boldsymbol{r}) \left(-\frac{1}{2}\nabla^2 + V(\boldsymbol{r}) \right) \Psi_\alpha(\boldsymbol{r}) + H_{\mathrm{int}}, \tag{1}$$

where $\Psi_{1,2}(\boldsymbol{r})$ is the fermion field operators of $A_{1,2}$ atoms, and we choose units for the Plank constant $\hbar$ and atomic mass m as $\hbar = 1$ and $m = 1$. At ultra-low temperature, the inter-atomic interaction part H_{int} in Eq. (1) becomes

$$H_{\mathrm{int}}^{(\mathrm{tc})} = g \int d\boldsymbol{r}\ \Psi_1^\dagger(\boldsymbol{r}) \Psi_2^\dagger(\boldsymbol{r}) \Psi_2(\boldsymbol{r}) \Psi_1(\boldsymbol{r}) \tag{2}$$

with the pseudo-potential of the low-energy s-wave scattering. Here we determine the coupling constant g in Eq. (2) with the s-wave scattering length a_{12} as $g = 4\pi a_{12}$, and neglect the inter-atomic interactions between same kinds of atoms because of the Pauli blocking effect. The trap potential $V(\boldsymbol{r})$ in Eq. (1) is a cylindrical harmonic oscillator potential,

$$V(\boldsymbol{r}) = \frac{1}{2}(\omega_c^2 r_c^2 + \omega_z^2 r_z^2), \tag{3}$$

where we introduce the Cartesian coordinates, $\boldsymbol{r} = (r_x, r_y, r_z)$, and $r_c^2 \equiv r_x^2 + r_y^2$, and assume the axial symmetry around the z-axis. In this paper, we call *longitudinal* and *transverse* directions for the parallel and orthogonal directions to the z-axis, respectively. Ratio of the trap frequencies, ω_c/ω_z, decides anisotropy of this system.

To simplify the model, we consider the symmetric two-component gases with same atomic densities, $\rho_1(\boldsymbol{r}, t) = \rho_2(\boldsymbol{r}, t) = \tilde{\rho}(\boldsymbol{r}, t)$, and use the time-dependent Hartree-Fock (HF) mean-field approximation [30]. In the HF approximation, the two-body interaction in Eq. (2) can be rewritten into a one-body interaction with the self-consistent mean-fields of the atomic densities, and the many-body effects are included in the mean-fields as mean-values. Then we can omit the subscripts for the atomic species by introducing a redefined system for the each component gas:

$$H = \int d\boldsymbol{r}\ \Psi^\dagger(\boldsymbol{r}) \left(-\frac{1}{2}\nabla^2 + V(\boldsymbol{r}) \right) \Psi(\boldsymbol{r}) + H_{\mathrm{int}} \tag{4}$$

with

$$H_{\rm int} \equiv g \int d\boldsymbol{r} \ \left(\Psi^\dagger(\boldsymbol{r}) \tilde{\rho}(\boldsymbol{r},t) \Psi(\boldsymbol{r}) - \frac{1}{2} (\tilde{\rho}(\boldsymbol{r},t))^2 \right), \tag{5}$$

where the atomic density, $\tilde{\rho}(\boldsymbol{r},t) = \left\langle \Psi^\dagger \Psi \right\rangle$, must be determined self-consistently. Here we should comment that symmetric l-component gases, l is an integer, take the same formulations in this paper with a renormalized coupling constant, $g \to (l-1)g$; thus the results in this paper can apply to any symmetric l-component gases.

In the HF approximation (Eqs. (4) and (5)), the ground state $\left|\Phi_0\right\rangle$ is given by the Slater determinant

$$\left|\Phi_0\right\rangle = \Big(\prod_{n \le n_{\rm F}} c_n^\dagger \Big) \left|{\rm vac}\right\rangle \tag{6}$$

with the fermion creation operator

$$c_n^\dagger \equiv \int d\boldsymbol{r} \ \Psi^\dagger(\boldsymbol{r}) \phi_n(\boldsymbol{r}), \tag{7}$$

where the normalized one-particle wave functions $\phi_n(\boldsymbol{r})$ are determined by the HF equations,

$$\left(-\frac{1}{2}\nabla^2 + V(\boldsymbol{r}) + g\rho(\boldsymbol{r}) \right) \phi_n(\boldsymbol{r}) = \epsilon_n \phi_n(\boldsymbol{r}), \tag{8}$$

where $\rho(\boldsymbol{r})$ is the atomic density in the ground state. The Fermi level $n_{\rm F}$ in Eq. (6) decide the atom number

$$N = \int d\boldsymbol{r} \ \rho(\boldsymbol{r}) = \int d\boldsymbol{r} \sum_{n \le n_{\rm F}} \left| \phi_n(\boldsymbol{r}) \right|^2 . \tag{9}$$

According to Eq. (6), the ground energy $E_{\rm g} \equiv \left\langle \Phi_0 \right| H \left| \Phi_0 \right\rangle$ becomes

$$E_{\rm g} = \int d\boldsymbol{r} \sum_{n \le n_{\rm F}} \phi_n^*(\boldsymbol{r}) \left(-\frac{1}{2}\nabla^2 + V(\boldsymbol{r}) \right) \phi_n(\boldsymbol{r}) + E_{\rm int} \tag{10}$$

with the interaction energy

$$E_{\rm int} \equiv \left\langle \Phi_0 \right| H_{\rm int} \left| \Phi_0 \right\rangle = \frac{g}{2} \int d\boldsymbol{r} \ (\rho(\boldsymbol{r}))^2. \tag{11}$$

The HF approximation is valid when the gases are weekly interacting and dilute, $g \sim 0$ and $|a_{12}| \ll \omega_{c,z}^{-1/2}$, as assumed in the present work. If the gases have strong correlations, e.g. the pair correlation in the BCS-BEC crossover [12] and the QLD correlations in the non-weekly interacting QLD systems [22], one should use another different method including the correlation effects. Furthermore, if the gases go to dense by deformation, the pseudo-potential in Eq. (2) for the 3D scattering may not be available because of the QLD scattering

effect. In this case, one should consider more realistic inter-atomic interactions instead of the pseudo-potential in Eq. (2). Those detailed discussions are beyond the purpose of this work, and omitted in this paper.

B. Breathing oscillations

The breathing oscillations are originally defined as compressive oscillations of fluids; especially, in spherical systems, they mean the monopole oscillations in the sense of the multipole expansion. However, in anisotropic systems, the monopole oscillations are inseparably mixed with incompressive oscillations (e.g. the quadrupole oscillations) [1], and we need to redefine the breathing oscillations as the mixtures of those oscillations as taken in this paper.

In the present work, we assume cylindrical deformation in excited gases according to the cylindrical trap potential in Eq. (3). Then the breathing oscillations appear in the expectation values of projected mean square radius operators

$$R_{c,z} \equiv \int d\boldsymbol{r}\ \Psi^{\dagger}(\boldsymbol{r}) r_{c,z}^{2} \Psi(\boldsymbol{r}). \tag{12}$$

In the actual experiments, those expectation values are directly observed with the absorption imaging method, and the excited gases are artificially generated with sudden change of the trap potentials.

When the variations of the expectation values of the $R_{c,z}$ in Eq. (12),

$$s_{c,z} \equiv \big\langle \Phi(t) \big| R_{c,z} \big| \Phi(t) \big\rangle - \big\langle \Phi_0 \big| R_{c,z} \big| \Phi_0 \big\rangle, \tag{13}$$

exhibit small amplitude oscillations, i.e. when the system shows the minimal breathing oscillations, we can describe these oscillations as

$$s_{c,z} = \sum_{\nu} C_{\nu} \big\langle \Phi_0 \big| R_{c,z} \big| \Phi_{\nu} \big\rangle e^{-iE_{\nu}t} + \text{c.c.} \tag{14}$$

with the time-evolving excited state

$$|\Phi(t)\rangle = |\Phi_0\rangle + \sum_{\nu} C_{\nu} \, |\Phi_{\nu}\rangle \, e^{-iE_{\nu}t}, \tag{15}$$

where we introduce the excited states $|\Phi_{\nu}\rangle$ with the excited energy E_{ν} and the minimal amplitudes C_{ν} determined by the initial condition. As shown in Eq. (14), those oscillations directly reflect the information of the ground and excited states. The oscillations of the $s_c(t)$

and $s_z(t)$ in Eq. (14) are called transverse and longitudinal oscillations, respectively, which correspond to the monopole oscillations when $s_c(t) = s_z(t)$ and the quadrupole oscillations when $s_c(t) = -s_z(t)/2$. In general, the transverse and longitudinal oscillations are coupled, so that one should consider the normal mode oscillations given by the normal mode operators $\tilde{R}_{c,z}$, which are described as linear combinations of $R_{c,z}$ and asymptotically correspond to $R_{c,z}$ at a decoupled limit. In the collective oscillations, the transition strength functions $\left|\langle\Phi_0|\tilde{R}_{c,z}|\Phi_\nu\rangle\right|^2$ are localized in a small range of the excited energy; then the corresponding normal mode oscillations behave like harmonic oscillations according to Eq. (14), and one can theoretically estimate the frequencies by using the scaling and sum-rule methods.

C. Scaling and sum-rule methods

We now formulate the scaling and sum-rule methods for the breathing oscillations of the fermion condensates, which are defined as the mixed oscillations of the $s_{c,z}$ in Eq. (13) as explained above.

According to Eq. (13), the behaviors of the breathing oscillations are determined from the time-dependent excited state $|\Phi(t)\rangle$. In the scaling method, the excited state is given by the scale transformation of the ground state $|\Phi_0\rangle$:

$$|\Phi(t)\rangle = e^{-i\xi_{\rm G}} e^{-(\lambda_c[H,R_c]+\lambda_z[H,R_z])/2}|\Phi_0\rangle \tag{16}$$

with the projected mean square radius operators $R_{c,z}$ defined in Eq. (12) and the Galilei transformation factor

$$e^{-i\xi_{\rm G}} \equiv e^{-i(\dot{\lambda}_c R_c + \dot{\lambda}_z R_z)/2}, \tag{17}$$

where $\dot{\lambda}_{c,z}$ represents the time derivative of $\lambda_{c,z}$. The scale parameters $\lambda_{c,z}(t)$ in Eq. (16) indicate the collective coordinates of the transverse and longitudinal oscillations, and are proportional to the projected mean square radius $s_{c,z}$ in Eq. (13) as a result.

In the HF approximation, the ground state is given by the Slater determinant in Eq. (6); then the excited state in Eq. (16) becomes

$$|\Phi(t)\rangle = \Big(\prod_{n\le n_{\rm F}} d_n^\dagger(t)\Big)|{\rm vac}\rangle \tag{18}$$

with

$$d_n^\dagger(t) \equiv \int d\boldsymbol{r}\ \Psi^\dagger(\boldsymbol{r})\tilde{\phi}_n(\boldsymbol{r},t), \tag{19}$$

where we introduce the scaled wave functions defined as

$$\tilde{\phi}_n(\boldsymbol{r},t) \equiv e^{-i(\dot{\lambda}_c r_c^2+\dot{\lambda}_z r_z^2)/2} e^{\lambda_c+\lambda_z/2} \phi_n\left(e^{\lambda_c}\boldsymbol{r}_c, e^{\lambda_z} r_z\right) \tag{20}$$

with $\boldsymbol{r}_c \equiv (r_x, r_y)$. These scaled wave functions satisfy the normalization and continuity conditions.

The time-dependent variational principle,

$$\delta \int dt \big\langle \Phi(t) \big| i\frac{d}{dt} - H \big| \Phi(t) \big\rangle \equiv \delta \int dt\ \mathcal{L}[\lambda, \dot{\lambda}] = 0, \tag{21}$$

gives the equations of motion of the scale parameters $\lambda_{c,z}(t)$ in Eq. (16). According to Eq. (18), the variational space in Eq. (21) is limited in the configuration space of the Slater determinants, so that the scaling method is in the time-dependent HF theory.

By substituting Eq. (18) into Eq. (21), the Lagrangian in Eq. (21) can be written as

$$\mathcal{L}[\lambda, \dot{\lambda}] = \sum_{j=c,z} \mathcal{M}_j^{(\lambda)} \dot{\lambda}_j^2 - \mathcal{H}, \tag{22}$$

where we define the mass parameters

$$\mathcal{M}_j^{(\lambda)} \equiv e^{-2\lambda_j} \mathcal{M}_j \tag{23}$$

with

$$\mathcal{M}_j \equiv \int d\boldsymbol{r}^3 r_j^2 \rho(r) \tag{24}$$

and the excited energy

$$\mathcal{H}[\lambda, \dot{\lambda}] \equiv \big\langle \Phi(t) \big| H \big| \Phi(t) \big\rangle - E_{\rm g} \tag{25}$$

with the ground energy $E_{\rm g}$ in Eq. (10). The excited energy in Eq. (25) is calculated as

$$\big\langle \Phi(t) \big| H \big| \Phi(t) \big\rangle = \frac{1}{2} \sum_{j=c,z} \mathcal{M}_j^{(\lambda)} \dot{\lambda}_j^2 + \mathcal{V}[\lambda] \tag{26}$$

with the potential parameter

$$\mathcal{V}[\lambda] \equiv \sum_{j=c,z} \left(e^{2\lambda_j} K_j + e^{-2\lambda_j} U_j\right) + e^{2\lambda_c+\lambda_z} E_{\rm int}, \tag{27}$$

where K_j and U_j are the kinetic and trap potential energies of the ground state in the j-direction motion,

$$K_j \equiv \int d\boldsymbol{r}\ \big\langle \Phi_0 \big| \Psi^\dagger(\boldsymbol{r}) \left(-\frac{1}{2}\nabla_j^2\right) \Psi(\boldsymbol{r}) \big| \Phi_0 \big\rangle \tag{28}$$

and

$$U_j \equiv \int d\boldsymbol{r}\ \left\langle \Phi_0 \middle| \Psi^\dagger(\boldsymbol{r}) \left(\frac{1}{2}\omega_j^2 r_j^2 \right) \Psi(\boldsymbol{r}) \middle| \Phi_0 \right\rangle. \tag{29}$$

In the present work, we study the minimal oscillations ($\lambda_{c,z} \ll 1$). To treat the minimal oscillations, we expand the excited energy in Eq. (25) by $\lambda_{c,z}$ and take the expanded terms up to the second order:

$$\mathcal{H}[\lambda, \dot{\lambda}] \simeq \frac{1}{2}\dot{\boldsymbol{\lambda}}^T B \dot{\boldsymbol{\lambda}} + \frac{1}{2}\boldsymbol{\lambda}^T C \boldsymbol{\lambda} \tag{30}$$

with $\boldsymbol{\lambda} \equiv (\lambda_c, \lambda_z)^T$, where the superscript T indicates the transposition. The B and C in Eq. (30) indicate the mass parameters,

$$B \equiv \begin{pmatrix} \mathcal{M}_c & 0 \\ 0 & \mathcal{M}_z \end{pmatrix}, \tag{31}$$

and the restoring forces,

$$C \equiv \begin{pmatrix} 4(K_c + U_c) + 4E_{\rm int} & 2E_{\rm int} \\ 2E_{\rm int} & 4(K_z + U_z) + E_{\rm int}, \end{pmatrix}, \tag{32}$$

respectively. Here one should note that the mass parameters B in Eq. (31) is diagonal because $\big[\big[H, R_c\big], R_z\big] = 0$ and $\big[\big[H, R_z\big], R_c\big] = 0$; in addition, the first order terms of λ in Eq. (30) must vanish owing to the virial theorem, which derives

$$K_c - \sum_{j=x,y} \int d\boldsymbol{r}\ \rho(\boldsymbol{r}) f_j(\boldsymbol{r}) = K_c - U_c + E_{\rm int} = 0 \tag{33}$$

and

$$K_z - \int d\boldsymbol{r}\ \rho(\boldsymbol{r}) f_z(\boldsymbol{r}) = K_z - U_z + \frac{1}{2}E_{\rm int} = 0 \tag{34}$$

with the virials

$$f_j(\boldsymbol{r}) \equiv \frac{r_j}{2}\frac{\partial}{\partial r_j}\left(V(\boldsymbol{r}) + g\rho(\boldsymbol{r})\right). \tag{35}$$

In order to diagonalize the $\mathcal{H}[\lambda, \dot{\lambda}]$ in Eq. (30), we introduce a complete set of orthonormal eigenvectors,

$$(B^{-1/2} C B^{-1/2})\boldsymbol{\eta}_j = \Omega_j^2 \boldsymbol{\eta}_j \tag{36}$$

for $j = c$ and z with the eigenvalues $\Omega_{c,z}$. Then the $\boldsymbol{\lambda}$ in Eq. (30) can be described as

$$\boldsymbol{\lambda} = B^{-1/2} \sum_{j=c,z} u_j \boldsymbol{\eta}_j \tag{37}$$

with

$$u_j = \boldsymbol{\eta}_j^T B^{1/2} \boldsymbol{\lambda}. \tag{38}$$

By substituting Eq. (37) into Eq. (30), the $\mathcal{H}$ in Eq. (30) can be written as the diagonal form,

$$\mathcal{H} = \frac{1}{2}\dot{\tilde{\boldsymbol{\lambda}}}^T \dot{\tilde{\boldsymbol{\lambda}}} + \frac{1}{2}\tilde{\boldsymbol{\lambda}}^T \tilde{C} \tilde{\boldsymbol{\lambda}} \tag{39}$$

with the normal mode vector $\tilde{\boldsymbol{\lambda}} \equiv (u_c, u_z)^T$ and the eigenvalue matrix

$$\tilde{C} \equiv \begin{pmatrix} \Omega_c^2 & 0 \\ 0 & \Omega_z^2 \end{pmatrix}. \tag{40}$$

According to Eq. (39), the $\Omega_{c,z}$ in Eq. (36) correspond to the collective frequencies of the normal modes. Using the normal mode representation, we obtain the decoupled scale transformation

$$\big|\Phi(t)\big\rangle = e^{-i(\dot{u}_c \tilde{R}_c + \dot{u}_z \tilde{R}_z)/2} e^{-(u_c \left[H, \tilde{R}_c\right] + u_z \left[H, \tilde{R}_z\right])/2} \big|\Phi_0\big\rangle \tag{41}$$

with the normal mode operators

$$\tilde{R}_j = \boldsymbol{\eta}_j^T B^{-1/2} \boldsymbol{R}, \tag{42}$$

where $\boldsymbol{R} = (R_c, R_z)^T$.

In principle, the scaling and sum-rule methods predict the same frequencies of the oscillations as shown in Appendix A. However the scaling method can describe an approximated time-evolution of the oscillations as shown in Eq. (16), and also give coupled oscillations with several modes, i.e. determination of the $\tilde{R}_j$ in Eq. (42), differently from the sum-rule method; on the other hand, the sum-rule method can describe more detailed information of the oscillations, e.g. collectivity of the oscillations, with additional data of the moments, differently from the scaling method. Thus the scaling and sum-rule methods have complementary roles to study the collective oscillations.

According to the above formulation of the scaling and sum-rule methods, behaviors of the breathing oscillations depend only on the parameters, $\mathcal{M}_{c,z}$, $K_{c,z}$, $U_{c,z}$, and $E_{\rm int}$, determined from the ground state properties. In fact, when these parameters are given, one can calculate the collective frequencies in Eq. (36) and predict the precise behaviors via the time-dependent excited state in Eq. (16) by solving the dynamical system in Eqs. (22) and (30).

III. GROUND STATE PROPERTIES

Let us calculate the parameters needed to predict the behaviors of the breathing oscillations in the scaling and sum-rule methods. These parameters are determined only from the ground state properties as explained in the previous section, and reflect the QLD shell-structures through the ground state properties. Thus we here consider the ground state properties and their QLD shell-structures by developing the semi-classical TFA to the super-anisotropic systems, and then determine the parameters by using this approach.

A. QLD shell-structures and extended TFA

The QLD shell-structures are defined as specific types of the shell-structures in the super-anisotropic systems. In general, the shell-structures can be well-defined in some asymptotic states, and it is useful for theoretical study to introduce such asymptotic states. Thus we here introduce the asymptotic states to study the QLD shell-structures. In the present work, we choose the non-interacting states ($g = 0$) for the asymptotic states and use the perturbation theory to include the inter-atomic interaction. The non-interacting asymptotic states implicitly have asymptotic variable-separation and corresponding asymptotic quantum numbers, so that the QLD shell-structures must be well-defined in the non-interacting asymptotic states and produce the QLD properties at the super-anisotropic limits in this framework.

According to the first order perturbation theory, all physical values are evaluated from the non-perturbative state, i.e. the ground state of the non-interacting gases ($g = 0$). In the non-interacting gases, the one-particle energies in Eq. (8) become

$$\epsilon_n = \sum_{j=x,y,z} \omega_j \left(n_j + \frac{1}{2} \right) \equiv \sum_{j=x,y,z} e_j \tag{43}$$

with $n = \{n_x, n_y, n_z\}$ and $\omega_x = \omega_y \equiv \omega_c$; the corresponding one-particle wave-functions $\phi_n(\boldsymbol{r})$ take the variable separation form:

$$\phi_n(\boldsymbol{r}) = \prod_{j=x,y,z} \varphi_j(r_j), \tag{44}$$

$$\varphi_j(r_j) = \frac{1}{\sqrt{2^{n_j} n_j!}} \left(\frac{\omega_j}{\pi} \right)^{1/4} e^{-\omega_j r_j^2/2} H_{n_j}(\sqrt{\omega_j} r_j), \tag{45}$$

with the Hermite functions $H_n(x)$. Here it should be noted that the asymptotic variable-separation and asymptotic quantum numbers are introduced in Eqs. (44) and (43), respectively.

In order to develop TFA, we here introduce the Wigner function defined as

$$f(\boldsymbol{r},\boldsymbol{p}) \equiv \int d\boldsymbol{s}\ e^{-i\boldsymbol{p}\cdot\boldsymbol{s}} \left\langle \Psi^\dagger\left(\boldsymbol{r}-\frac{\boldsymbol{s}}{2}\right)\Psi\left(\boldsymbol{r}+\frac{\boldsymbol{s}}{2}\right)\right\rangle. \tag{46}$$

Then the expectation value of a one-body operator

$$A = \int d\boldsymbol{r}\ \Psi^\dagger(\boldsymbol{r})\, a(\hat{\boldsymbol{r}},\hat{\boldsymbol{p}})\Psi(\boldsymbol{r}) \tag{47}$$

becomes

$$\langle A\rangle = \frac{1}{(2\pi)^3}\int d\boldsymbol{r}\int d\boldsymbol{p}\ a^{(\mathrm{cl})}(\boldsymbol{r},\boldsymbol{p}) f(\boldsymbol{r},\boldsymbol{p}) \tag{48}$$

with the Weyl classical function $a^{(\mathrm{cl})}(\boldsymbol{r},\boldsymbol{p})$ corresponding to the quantum mechanical operator $a(\hat{\boldsymbol{r}},\hat{\boldsymbol{p}})$. In the non-interacting gases, the Wigner function becomes

$$f(\boldsymbol{r},\boldsymbol{p}) = \sum_n \mathcal{F}(\epsilon_n) \prod_{j=x,y,z} f_j(r_j,p_j;e_j) \tag{49}$$

according to Eqs. (43) and (44), where we define

$$f_j(r_j,p_j;e_j) \equiv \int ds\ e^{-ip_j s}\varphi_j^*\left(r_j-\frac{s}{2}\right)\varphi_j\left(r_j+\frac{s}{2}\right) \tag{50}$$

and use the zero-temperature Fermi distribution function $\mathcal{F}(\epsilon_n) = \Theta(e_{\mathrm{F}}-\epsilon_n)$ in Eq. (49) with the Fermi energy e_{F} and the Heaviside's step function $\Theta(x)$. The Wigner function in Eq. (49) is simplified in TFA by smoothing the energy-level density.

1. Conventional TFA

The conventional 3DTFA, explained in Appendix B, is valid only when the anisotropy of the trap is not so large; otherwise 3DTFA loses the validity owing to the QLD shell-structures. In fact, this proposition is clearly demonstrated in the one-particle energy-level densities [31]. We now show them in the oblate and prolate deformed traps in order.

First we consider the oblate deformed potentials ($\omega_z > \omega_c$). Here we take the anisotropy $a_z \equiv \omega_z/\omega_c$ to be an integer to simplify expressions. At that time, the energy-level density can be defined as the mean value of the number of energy-levels in an energy width ω_c

associated with an energy eigenvalue $e_q \equiv \omega_c q_c + e_0$, where we introduce the quantum number q_c for the c-direction motion and the zero point energy $e_0 \equiv \omega_c + \omega_z/2$. It becomes

$$D(e_q) = \frac{(q_z+1)(2q_c+2-a_z q_z)}{2\omega_c} \tag{51}$$

with the maximum quantum number $q_z \equiv \mathrm{int}((e_q - e_0)/\omega_z)$ for the z-direction motion, where the round-down function $\mathrm{int}(x)$ returns the integer part of x.

By smoothing the energy level density in Eq. (51) with $q_{c,z} \approx (\varepsilon - e_0)/\omega_{c,z}$, we obtain

$$D(\varepsilon) \approx D^{(3)}(\varepsilon) \equiv \frac{\varepsilon^2}{2\omega_c^2 \omega_z} \Theta(\varepsilon), \tag{52}$$

where $D(\varepsilon)$ agrees with that in 3DTFA (see Eq. (B7)). According to the smoothing method, this agreement is approved only when the energy level density in $e_q \gg \omega_z > \omega_c$ principally contribute to the system, i.e. the anisotropy of the trap is not large; otherwise the QLD shell-structures have non-negligible influence.

In fact, when we consider the super-anisotropic limit, the energy level density at $q_z = 0$ ($\omega_z > e_q \gg \omega_c$) principally contribute to the system; then, by smoothing the energy level density in Eq. (51) only with $q_c \approx (\varepsilon - e_0)/\omega_c$, we obtain

$$D(\varepsilon) \approx D^{(2)}(\varepsilon) \equiv \frac{1}{\omega_c^2} \left(\varepsilon - \frac{\omega_z}{2}\right) \Theta\left(\varepsilon - \frac{\omega_z}{2}\right), \tag{53}$$

where $D(\varepsilon)$ agrees with that in 2DTFA (see Eq. (B7)).

In Fig. 1, we show the energy level densities when $\omega_z/\omega_c = 21$. When $\varepsilon \gg \omega_z$, $D(e_q)$ (the open circles) approximately agrees with $D^{(3)}(\varepsilon)$ (the dashed line) as described in Eq. (52); otherwise they have some difference reflecting the QLD shell-structures. When $\varepsilon < 31.5\,\omega_c = (3/2)\omega_z$ ($q_z = 0$), $D(e_q)$ (the open circles) agrees with $D^{(2)}(\varepsilon)$ (the solid line) as described in Eq. (53).

Second we consider the prolate deformed potentials ($\omega_c > \omega_z$). Here we also take the anisotropy $a_c \equiv \omega_c/\omega_z$ to be an integer. At that time, we can use the same way in the oblate deformed potentials with exchange of the subscripts ($c \leftrightarrow z$) to obtain the energy-level density; it becomes

$$D(e_q) = \frac{(q_c+1)(q_c+2)}{2\omega_z}. \tag{54}$$

According to the same way in the oblate deformed potentials, the energy level density in Eq. (54) agrees with that in 3DTFA, $D^{(3)}(\varepsilon)$, when the anisotropy of the trap is not so

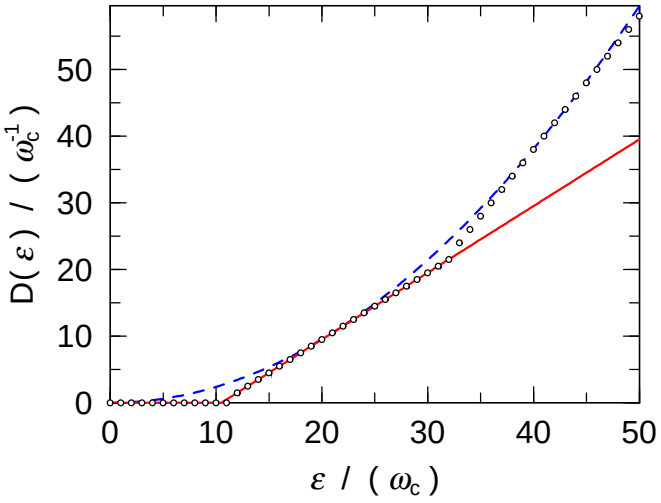

FIG. 1: (color online) The energy level densities when $\omega_z/\omega_c = 21$. The open circles represent the values of $D(e_q)$; the dashed and solid lines correspond to the results in 3DTFA and 2DTFA, respectively.

large; otherwise they disagree owing to the QLD shell-structures. Especially, at the super-anisotropic limit ($q_c = 0$ and $\omega_c > e_q \gg \omega_z$), the energy level density in Eq. (54) can be written as

$$D(\varepsilon) \approx D^{(1)}(\varepsilon) \equiv \frac{1}{\omega_z}\Theta\left(\varepsilon - \omega_c\right) \tag{55}$$

by smoothing $q_z \approx (\varepsilon - e_0)/\omega_z$, where $D(\varepsilon)$ agrees with that in 1DTFA (see Eq. (B7)).

In Fig. 2, we show the energy level density when $\omega_c/\omega_z = 21$. When $\varepsilon \gg \omega_c$, $D(e_q)$ (the open circles) approximately agrees with $D^{(3)}(\varepsilon)$ (the dashed line) as same as that in the oblate deformed potentials. When $\varepsilon < 42\ \omega_z = 2\omega_c$ ($q_c = 0$), $D(e_q)$ (the open circles) agrees with $D^{(1)}(\varepsilon)$ (the solid line) as described in Eq. (55). The appearance of the QLD shell-structures in the prolate deformed systems is clearer than that in the oblate deformed systems.

Here it should be noted that the QLD shell-structures exhibit the hierarchic structures associated with the maximum quantum numbers for the narrow direction motions, q_z and q_c, in the both cases of the oblate and prolate deformed potentials as shown in Figs. 1 and 2, respectively. The appearance of those hierarchic structures is a specific feature of the QLD shell-structures, and also shown in the following results. In general, we can define the QLD shell-structures as the hierarchic structures in one-particle energy-level densities

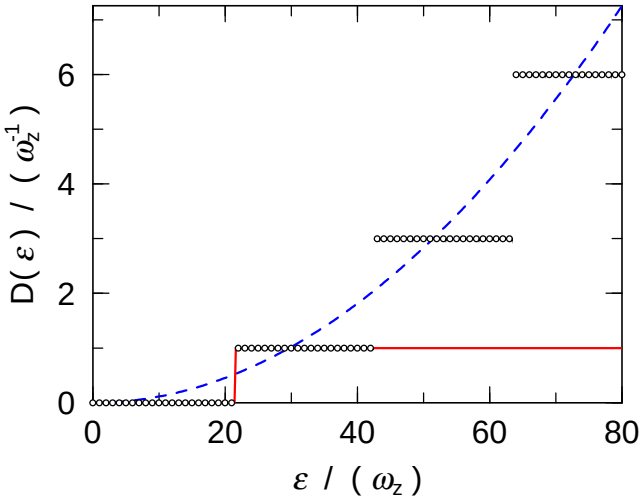

FIG. 2: (color online) The energy level densities when $\omega_c/\omega_z = 21$. The open circles represent the values of $D(e_q)$; the dashed and solid lines correspond to the results in 3DTFA and 1DTFA, respectively.

in asymptotic states, where one-particle wave-functions can be denoted as product of two wave-functions with different energy-levels and asymptotic quantum numbers (i.e. fine and coarse modes) [35].

2. Extended TFA

As shown in the energy-level densities, the conventional 3DTFA should not be applied to the super-anisotropic systems owing to the QLD shell-structures. We here introduce a new approach to develop TFA to the super-anisotropic systems.

In order to take into account the QLD shell-structures, we smooth the Wigner function in Eq. (49) only for the c-direction in the oblate deformed potentials and for the z-direction in the prolate deformed potentials:

$$f(\boldsymbol{r},\boldsymbol{p}) = \int_0^\infty d\varepsilon\; G^{(j)}(\varepsilon) \tag{56}$$

with

$$G^{(2)}(\varepsilon) \equiv \mathcal{F}\left(\varepsilon + e^{(2)}_{\rm cl}(\boldsymbol{r}_c,\boldsymbol{p}_c)\right) \sum_{n_z} \delta\left(\varepsilon - e_z\right) f_z(r_z,p_z;e_z) \tag{57}$$

in the oblate deformed potentials ($j = 2$) and

$$G^{(1)}(\varepsilon) \equiv \mathcal{F}\left(\varepsilon + e_{\rm cl}^{(1)}(r_z, p_z)\right) \sum_{n_x,n_y} \delta\left(\varepsilon - e_x - e_y\right) \prod_{j=x,y} f_j(r_j, p_j; e_j) \tag{58}$$

in the prolate deformed potentials ($j = 1$), where we introduce the two and one dimensional classical energies, $e_{\rm cl}^{(2)}(\boldsymbol{r}_c, \boldsymbol{p}_c) \equiv p_c^2/2 + \omega_c^2 r_c^2/2$ and $e_{\rm cl}^{(1)}(r_z, p_z) \equiv p_z^2/2 + \omega_z^2 r_z^2/2$.

Here it should be noted that the Wigner function in Eq. (56) agrees with that in 3DTFA,

$$f^{(3)}(\boldsymbol{r}, \boldsymbol{p}) \equiv \mathcal{F}\left(e_{\rm cl}(\boldsymbol{r}, \boldsymbol{p})\right) \tag{59}$$

with $e_{\rm cl}(\boldsymbol{r}, \boldsymbol{p}) \equiv p^2/2 + V(\boldsymbol{r})$, when $\varepsilon \gg \omega_c, \omega_z$; thus we can rewrite the Wigner functions in Eq. (56) as

$$f(\boldsymbol{r}, \boldsymbol{p}) = \int_0^{\varepsilon_{\rm c}} d\varepsilon\ G^{(j)}(\varepsilon) + f^{(3)}(\boldsymbol{r}, \boldsymbol{p}) \Theta\left(e_{\rm cl}(\boldsymbol{r}, \boldsymbol{p}) - \varepsilon_{\rm c}\right) \tag{60}$$

in the oblate ($j = 2$) and prolate ($j = 1$) deformed potentials with a large cutoff energy $\varepsilon_{\rm c}$. In this paper, we call the rewritten form of the Wigner function in Eq. (60) as *extended TFA* (ETFA), which agrees with the original Wigner function in Eq. (56) when $\varepsilon_{\rm c} > e_{\rm F}$.

The hierarchic structures can also be seen in Eq. (60) through Eqs. (57) and (58), so that ETFA must reproduce the QLD shell-structures below the cutoff energy; above the cutoff energy, ETFA have no shell-structure as shown in Eq. (59). However, pragmatically, it is no need to treat the QLD shell-structures in all range of the energy-level density because the QLD shell-structures have non-negligible influence only in the low-energy range. In fact, the results in ETFA with finite cutoff energies show good agreement with those in the exact calculations ($\varepsilon_{\rm c} \to \infty$) as demonstrated in the next section.

3. Fermi energy and crossover behaviors

The QLD shell-structures in Eq. (56) affect physical values in the super-anisotropic systems. Here we show the Fermi energy $e_{\rm F}$ for an example. The Fermi energy is determined by the particle number condition,

$$N = \frac{1}{(2\pi)^3} \int d\boldsymbol{r} \int d\boldsymbol{p}\ f(\boldsymbol{r}, \boldsymbol{p}) \tag{61}$$

with the Wigner function in Eq. (60). In particular, we obtain

$$e_{\rm F}^{(d)} = \left(d! \left(\prod_{j=1}^{d} \omega_j\right) N\right)^{1/d} + e_0^{(d)} \tag{62}$$

in the d-dimensional TFA with the zero-point energy shift, $e_0^{(1)} = \omega_c$, $e_0^{(2)} = \omega_z/2$, and $e_0^{(3)} = 0$, according to Eqs. (52), (53), and (55) (generally Eq. (B7)).

In Fig. 3, we show the Fermi energies in the oblate and prolate deformed potentials when $N = 10^4$ and 10^3, respectively. When the anisotropy of the trap is not so large, the exact values of the Fermi energy (the open circles) approximately agrees with that in 3DTFA (the short-dashed lines); as the anisotropy increases, it shows crossover behavior from that in 3DTFA to 2DTFA or 1DTFA and exactly agrees with that in 2DTFA (the long-dashed line in Fig. 3a) when $e_{\rm F} = (3/2)\omega_z$ and $N = (\omega_z/\omega_c)^2/2$ in the oblate deformed potentials and in 1DTFA (the long-dashed line in Fig. 3b) when $e_{\rm F} = 2\omega_c$ and $N = \omega_c/\omega_z$ in the prolate deformed potentials . Here one should note the results in ETFA (the solid lines), which include the QLD shell-structures only below $\varepsilon = (3/2)\omega_z$ or $\varepsilon_{\rm c} = 2\omega_c$, i.e. the lowest shell state ($q_z = 0$ or $q_c = 0$), as shown in Eq. (60). These results roughly reproduce the global crossover behaviors and slightly different from the exact calculations in the middle range of the anisotropy owing to the effect of the upper QLD shell-structures with the hierarchic structures.

As shown in the behavior of the Fermi energy in Fig. 3, the QLD shell-structures induce the crossover behavior between the 3DTF and 2/1DTF gases. The crossover behavior is an important feature of the trapped quantum gases. The phase diagrams of the weekly interacting Fermi gases can be determined by the ratio of $e_{\rm F}$ and $\omega_{z,c}$ ($\gg \omega_{c,z}$) according to the dimensional analysis. We briefly describe it in Fig. 4.

B. Determination of the parameters

Using ETFA, we now decide the parameters needed in the scaling and sum-rule methods. According to the perturbation theory, we expand these parameters by the coupling constant g and take the zero-th and first order terms: e.g. $K_j \simeq K_{j0} + K_{j1}$ and $U_j \simeq U_{j0} + U_{j1}$ for $j = c$ and z.

According to the Wigner functions in Eq. (56), the zero-th order terms of the potential energies in the c and z-direction motion, U_{c0} and U_{z0}, become

$$U_{c0} = \sum_{n_z=0}^{\infty} \frac{(e_{\rm F} - e_z)^3}{6\omega_c^2} \Theta\left(e_{\rm F} - e_z\right), \tag{63}$$

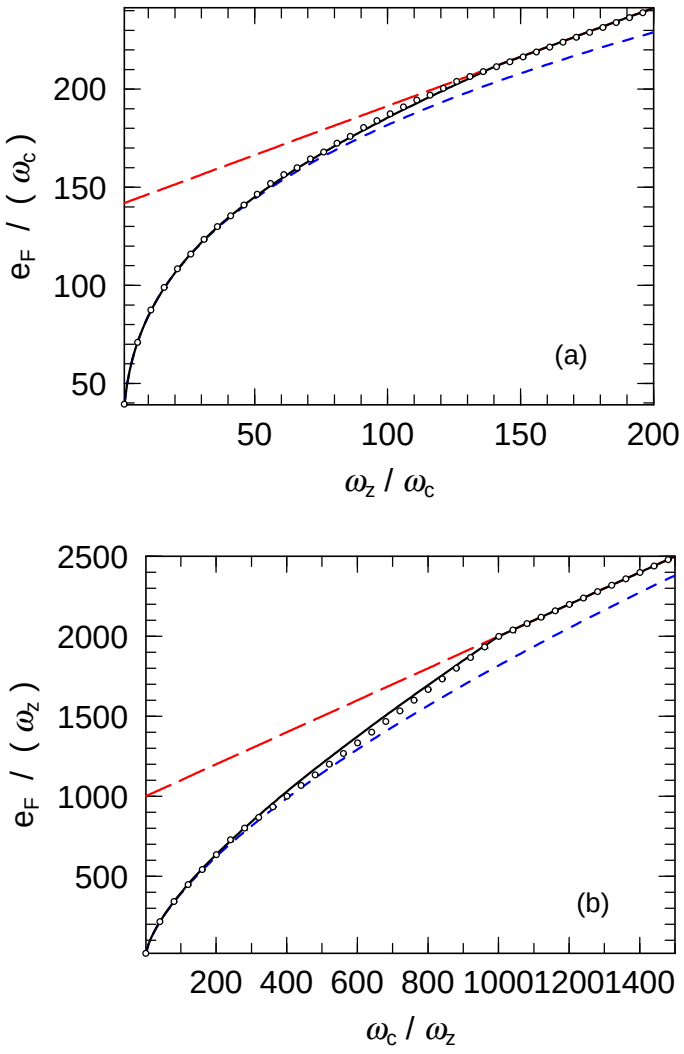

FIG. 3: (color online) The Fermi energies in the oblate deformed potentials when $N = 10^4$ (a) and in the prolate deformed potentials when $N = 10^3$ (b). The open circles represent the exact results; the solid, short-dashed, and long-dashed lines represent the results in ETFA ($\varepsilon_c = (3/2)\omega_z$ (a) or $2\omega_c$ (b)), 3DTFA, and 2DTFA (a) or 1DTFA (b), respectively.

$$U_{z0} = \sum_{n_z=0}^{\infty} \frac{e_z(e_F - e_z)^2}{4\omega_c^2} \Theta\left(e_F - e_z\right) \tag{64}$$

in the oblate deformed potentials and

$$U_{c0} = \sum_{n_x=0}^{\infty} \sum_{n_y=0}^{\infty} \frac{e_c(e_F - e_c)}{2\omega_z} \Theta\left(e_F - e_c\right), \tag{65}$$

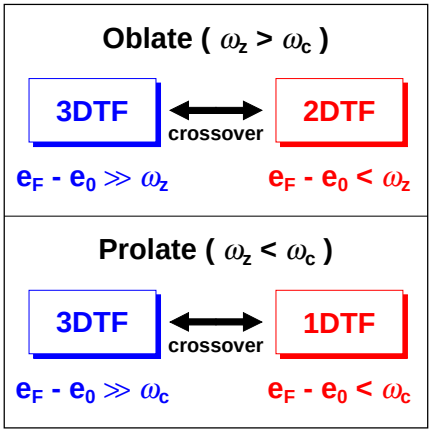

FIG. 4: (color online) The phase diagrams of the weekly interacting Fermi gases in the anisotropic traps.

$$U_{z0} = \sum_{n_x=0}^{\infty} \sum_{n_y=0}^{\infty} \frac{(e_{\rm F} - e_c)^2}{4\omega_z} \Theta\left(e_{\rm F} - e_c\right) \tag{66}$$

in the prolate deformed potentials, where we use the e_z and $e_c \equiv e_x + e_y$ in Eq. (43) and the integral formulas of the Hermite functions. By smoothing the residual sums in Eqs. (63)-(66), $\sum_{n_j} \to \int de_j/\omega_j$ $(j = x, y, z)$, we obtain the results in 3DTFA:

$$U_{c0}^{(3)} = 2U_{z0}^{(3)} = \frac{1}{4}(6\omega_z\omega_c^2 N^4)^{1/3}. \tag{67}$$

By taking $n_z = 0$ and $n_x = n_y = 0$ in the residual sums in Eqs. (63)-(66), we obtain the results in 2DTFA and 1DTFA, respectively:

$$U_{c0}^{(2)} = \frac{\sqrt{2}}{3}\omega_c N^{3/2}, \quad U_{z0}^{(2)} = \frac{\omega_z}{4}N \tag{68}$$

and

$$U_{c0}^{(1)} = \frac{\omega_c}{2}N, \quad U_{z0}^{(1)} = \frac{\omega_z}{4}N^2. \tag{69}$$

In Fig. 5, we show the zero-th order terms of the potential energies U_{c0} and U_{z0} in Eqs. (63)-(66) in the oblate deformed potentials when $N = 10^4$ and in the prolate deformed potentials when $N = 10^3$, respectively. The crossover behavior and the QLD shell-structures also appear in these plots.

The mass parameters in Eq. (31) is determined by the potential energies owing to the definitions:

$$\mathcal{M}_{c,z} = \frac{2}{\omega_{c,z}^2} U_{c,z}. \tag{70}$$

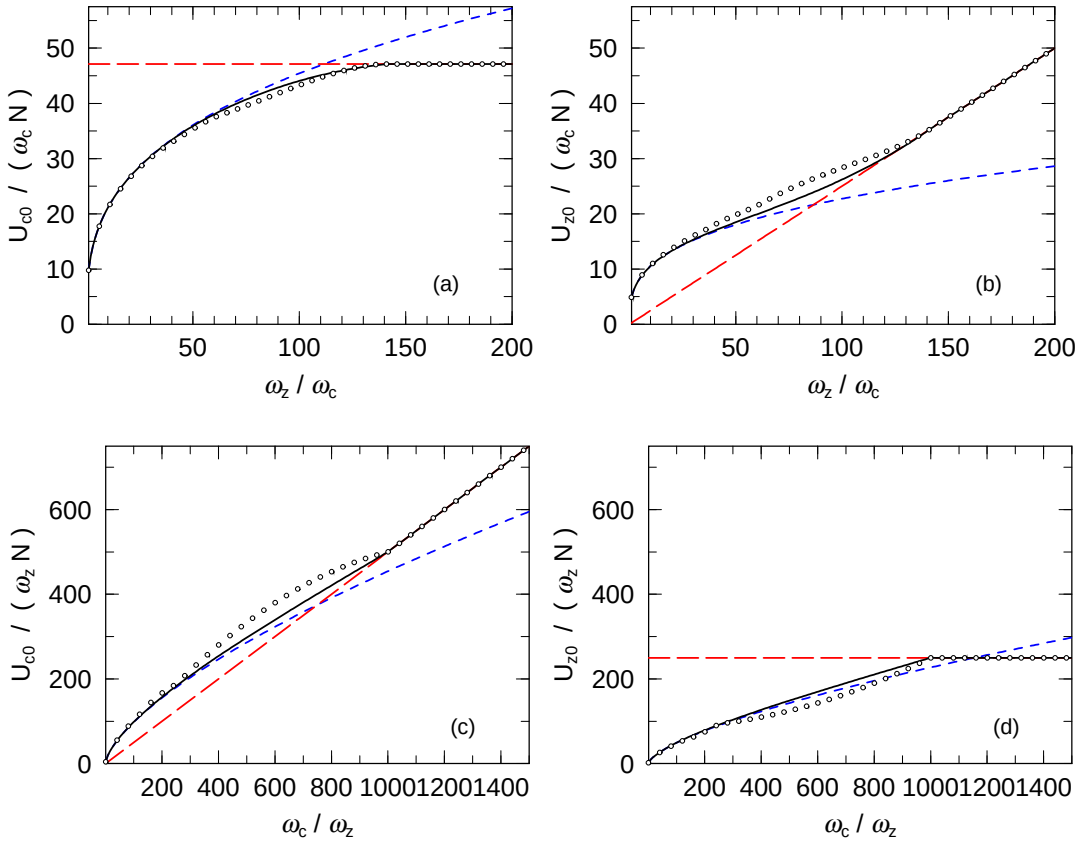

FIG. 5: (color online) The potential energies, U_{c0} [(a) (c)] and U_{z0} [(b) (d)], in the oblate deformed potentials when $N = 10^4$ [(a) (b)] and in the prolate deformed potentials when $N = 10^3$ [(c) (d)]. The open circles represent the exact results; the solid, short-dashed, and long-dashed lines represent the results in ETFA ($\varepsilon_c = (3/2)\omega_z$ [(a) (b)] or $2\omega_c$ [(c) (d)]), 3DTFA, and 2DTFA [(a) (b)] or 1DTFA [(c) (d)], respectively.

The zero-th order terms of the kinetic energies equal those of the potential energies according to the virial theorem in Eqs. (33) and (34):

$$K_{j0} = U_{j0} \tag{71}$$

for $j = c$ and z.

In the first order terms, the perturbation theory gives

$$K_{j1} = -U_{j1} \tag{72}$$

for $j = c$ and z owing to the variable separation of the noninteracting ground state; further-

more, the virial theorem in Eqs. (33) and (34) gives

$$E_{\rm int} = U_{c1} - K_{c1} = 2(U_{z1} - K_{z1}). \tag{73}$$

According to Eqs. (72) and (73), we obtain the first order terms:

$$U_{c1} = -K_{c1} = \frac{1}{2}E_{\rm int}, \quad U_{z1} = -K_{z1} = \frac{1}{4}E_{\rm int}. \tag{74}$$

The interaction energy $E_{\rm int}$ in the crossover process varies between those in the d-dimensional TFA,

$$E_{\rm int}^{(d)} = 4\beta^{(d)} g\sqrt{\omega_z \omega_c^2 N^3}, \tag{75}$$

where $\beta^{(3)} \equiv 128\sqrt{3}/(945\pi^3) \approx 0.00756$, $\beta^{(2)} \equiv 1/(24\pi^{3/2}) \approx 0.00748$, and $\beta^{(1)} \equiv \sqrt{2}/(6\pi^3) \approx 0.00760$. Owing to $\beta^{(3)} \approx \beta^{(2)} \approx \beta^{(1)}$, the $E_{\rm int}^{(d)}$ in Eq. (75) are nearly same values, so that the interaction energy has little influence on the QLD shell-structures, and we approximate it as

$$E_{\rm int} \approx E_{\rm int}^{(3)} \tag{76}$$

in the following sections.

IV. BEHAVIORS OF THE BREATHING OSCILLATIONS

We here show the calculational results by using the parameters determined in the previous section. Firstly we calculate the normal mode frequencies of the breathing oscillations in the scaling and sum-rule methods. Next we demonstrate the time-evolution in the present framework.

A. Normal mode frequencies

According to the eigen-equations (Eq. (36)) with Eqs. (31) and (32), we obtain the normal mode frequencies of the breathing oscillations, $\Omega_{c,z}$, up to the first order of the interaction energy as

$$\Omega_j = 2\sqrt{\frac{(K_j + U_j)}{\mathcal{M}_j}} + \alpha_j \sqrt{\frac{1}{\mathcal{M}_j (K_j + U_j)}} E_{\rm int} + O(E_{\rm int}^2) \tag{77}$$

for $j = c$ and z, where $\alpha_c \equiv 1$ and $\alpha_z \equiv 1/4$. These solutions are also expanded by the coupling constant g: $\Omega_j \simeq \Omega_{j0} + \Omega_{j1}$, where

$$\Omega_{j0} = 2\sqrt{\frac{(K_{j0} + U_{j0})}{\mathcal{M}_{j0}}}, \tag{78}$$

and

$$\Omega_{j1} = \frac{\Omega_{j0}}{2}\left(\frac{K_{j1} + U_{j1}}{K_{j0} + U_{j0}} - \frac{\mathcal{M}_{j1}}{\mathcal{M}_{j0}} + \frac{\alpha_j E_{\rm int}}{K_{j0} + U_{j0}}\right). \tag{79}$$

The zero-th order terms correspond to those of the noninteracting gases. By substituting Eqs. (70) and (71) into Eq. (78), we obtain

$$\Omega_{j0} = 2\omega_j. \tag{80}$$

This result only depends on the trap frequencies and does not be affected by the QLD shell-structures.

The first order terms are also obtained as

$$\Omega_{c1} = 0, \quad \Omega_{z1} = -\frac{\omega_z}{8}\frac{E_{\rm int}}{U_{z0}} \tag{81}$$

by substituting Eqs. (70), (71), and (74) into Eq. (79). This result reveals that the interaction and QLD shell-structures affect only the frequency of the longitudinal normal mode, but not that of the transverse normal mode. The vanishment in the transverse normal mode reflects a typical phenomenon of the transverse mode because the mixing, i.e. the off-diagonal elements in Eq. (32), has no influence on the first order terms in Eq. (81).

According to Eq. (81), the QLD shell-structures contribute the frequency of the longitudinal normal mode principally through the potential energy U_{z0} because Eq. (81) contains only the two parameters, U_{z0} and $E_{\rm int}$, and the QLD shell-structures have little influence on the interaction energy $E_{\rm int}$ as shown in Eq. (76). Thus the frequency of the longitudinal normal mode exhibits the crossover behaviors associated with those of the potential energy U_{z0} as shown in Fig. 5. At the d-dimensional TFA limits (Eqs. (67)-(69)), the corresponding frequency $\Omega_{z1}^{(d)}$ becomes

$$\Omega_{z1}^{(3)} = -\frac{1}{6^{1/3}}\left(\frac{\omega_z}{\omega_c}\right)^{2/3}\frac{E_{\rm int}}{N^{4/3}}, \tag{82}$$

$$\Omega_{z1}^{(2)} = -\frac{1}{2}\frac{E_{\rm int}}{N}, \tag{83}$$

and

$$\Omega_{z1}^{(1)} = -\frac{1}{2}\frac{E_{\rm int}}{N^2}. \tag{84}$$

In Fig. 6, we show the first order term in the frequency of the longitudinal normal mode, Ω_{z1}, in Eq. (81) by using the parameters in Eqs. (64), (66), and (76). Here one can see the crossover behaviors in the exact results (the open circles) between the results in 3DTFA (the short-dashed lines) and 2DTFA (a) or 1DTFA (b) (the long-dashed lines).

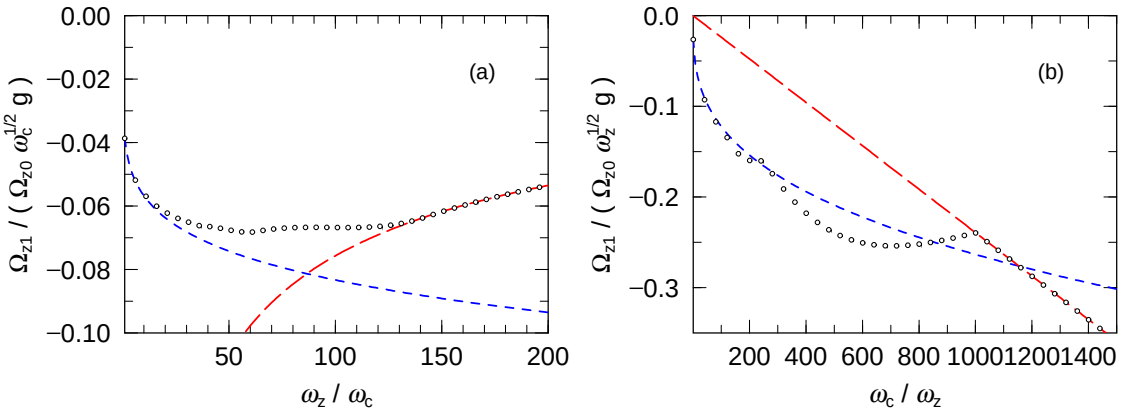

FIG. 6: (color online) The first order term in the longitudinal normal mode frequency, Ω_{z1}, in the oblate deformed potentials when $N = 10^4$ (a) and in the prolate deformed potentials when $N = 10^3$ (b). The open circles represent the exact results. The short-dashed and long-dashed lines represent the results in 3DTFA and 2DTFA (a) or 1DTFA (b), respectively.

In Fig. 7, we show comparison between the exact results in Fig. 6 (the open circles) and the results in ETFA at $\varepsilon_c = (3/2)\omega_z$, $(5/2)\omega_z$, and $(7/2)\omega_z$ (a) or $2\omega_c$, $3\omega_c$, and $4\omega_c$ (b) (the short-dashed, long-dashed, and solid lines, respectively). There appear three ranges reflecting the hierarchic structures: (i) $\omega_z/\omega_c > \sqrt{2N}$ (a) or $\omega_c/\omega_z > N$ (b). (ii) $\sqrt{2N} > \omega_z/\omega_c > \sqrt{(2/5)N}$ (a) or $N > \omega_c/\omega_z > N/4$ (b). (iii) $\sqrt{(2/5)N} > \omega_z/\omega_c$ (a) or $N/4 > \omega_c/\omega_z$ (b).

In range (i), the exact results agree with those in 2DTFA (a) or 1DTFA (b), so that all results in ETFA reproduce the exact values.

In range (ii), the QLD shell-structures below the first shell-structure only contribute to the exact results. Thus the results in ETFA at $\varepsilon_c \geq (5/2)\omega_z$ (a) or $3\omega_c$ (b) can only reproduce the exact values. The difference between the results in exact calculations and ETFA at $\varepsilon_c = (3/2)\omega_z$ (a) or $2\omega_c$ (b) indicates the effect of the QLD shell-structures of the first shell-structure.

In range (iii), the QLD shell-structures below the second shell-structure only contribute

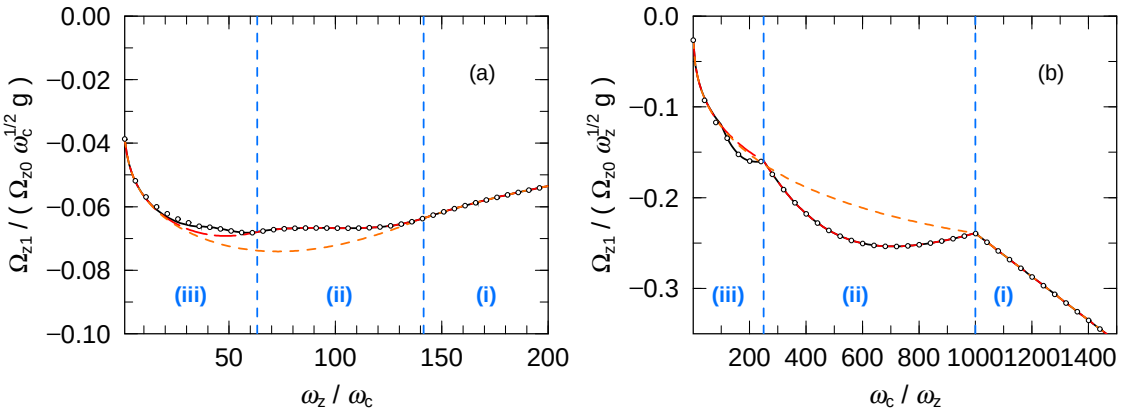

FIG. 7: (color online) Same as Fig. 6, but the short-dashed, long-dashed, and solid lines represent the results in ETFA at $\varepsilon_c = (3/2)\omega_z$, $(5/2)\omega_z$, and $(7/2)\omega_z$ (a) or $2\omega_c$, $3\omega_c$, and $4\omega_c$ (b), respectively.

to the results. Thus the results in ETFA at $\varepsilon_c \geq (7/2)\omega_z$ (a) or $5\omega_c$ (b) can only reproduce the exact values. There are additional detailed structures associated with the hierarchic structures; however it is difficult to find them up in Fig. 7 because the difference between the results in exact calculations and ETFA is visually small.

Finally we comment on the particle number dependence on the above results. When the particle number varies, there principally appear two kinds of quantitative change. One is the change of the values at the 2DTF and 1DTF limit as shown in Eqs. (82)-(84): $\Omega_{z1}^{(3)} \propto N^{1/6}$, $\Omega_{z1}^{(2)} \propto N^{1/2}$, and $\Omega_{z1}^{(1)} \propto N^{-1/2}$. The other is the change of the critical anisotropy points between the ranges (i) and (ii), which are proportional to $N^{1/2}$ for the oblate deformed potentials and to N for the prolate deformed potentials.

B. Time-evolution

We here show the results of the time-evolution in the present framework by using the parameters determined in the previous section.

In the scaling method, the collective coordinates $\lambda_{c,z}(t)$ determine the behaviors of the breathing oscillations as described in Eq. (16). In order to observe the collective coordinates, it is useful to measure the projected mean square radius $s_{c,z}(t)$ defined in Eq. (13), which are proportional to $\lambda_{c,z}(t)$. We here demonstrate the time-evolution of $s_{c,z}(t)$ ($\propto \lambda_{c,z}(t)$) by solving the dynamical system (Eqs. (22) and (30)) in the classical mechanics [36]; the

equations of motion, up to the first order of the the interaction energy $E_{\rm int}$, become

$$\frac{d^2\lambda_c}{dt^2} = -\Omega_c^2(\lambda_c - \gamma_c\lambda_z) \tag{85}$$

and

$$\frac{d^2\lambda_z}{dt^2} = -\Omega_z^2(\lambda_z - \gamma_z\lambda_c) \tag{86}$$

with

$$\gamma_{c,z} \equiv -\frac{\omega_{c,z}^2}{\Omega_{c,z}^2}\frac{E_{\rm int}}{U_{c,z}}. \tag{87}$$

In Fig. 8, we show the time evolution of the collective coordinates of the transverse and longitudinal oscillations, $s_c(t)$ and $s_z(t)$, in the oblate deformed potential ($\omega_z/\omega_c = 80$) when $N = 10^4$ and in the prolate deformed potential ($\omega_c/\omega_z = 600$) when $N = 10^3$. Here we choose an initial condition, $s_c(t=0) = s_z(t=0) = s_0$ and $\dot{s}_c(t=0) = \dot{s}_z(t=0) = 0$, which correspond to an experimental situation by sudden change of the trap frequency at $t = 0$. The short-dashed lines represent the results of the non-interacting gases ($g = 0$); the solid lines and the dotted separations represent the results and the periods of the normal modes (Eqs. (80) and (81)) when $g = 0.3\omega_c^{-1/2}$ for the oblate case and $g = 0.2\omega_z^{-1/2}$ for the prolate case, respectively.

As shown in Fig. 8, the inter-atomic interaction principally induces two kinds of influence: frequency decrement in the longitudinal oscillations (Fig. 8b and 8d) and shift of the center position of the faster oscillations (Fig. 8b and 8c).

The frequency decrements are confirmed from the agreements of the frequencies in the results and the corresponding normal mode frequencies as shown in Fig. 8 (the solid lines and dotted separations) and Eqs. (85) and (86); according to Eq. (81), the inter-atomic interaction keeps the normal mode frequencies in the transverse oscillations, and reduces (increases) those in the longitudinal oscillations when $g > 0$ (< 0), so that the frequency decrements occur only in the longitudinal oscillations.

The center shifts in the faster oscillations are induced by the mixing of the faster and slower oscillations. The mixing effects of the faster oscillations on the slower oscillations vanish owing to the coarse graining in the long time scales corresponding to the periods of the slower oscillations [37]; however the mixing effects of the slower oscillations on the faster oscillations remain as the center shifts, which are nearly constant in the small time scales and exhibit beat structures in the long time scales. The center shifts can also be seen in

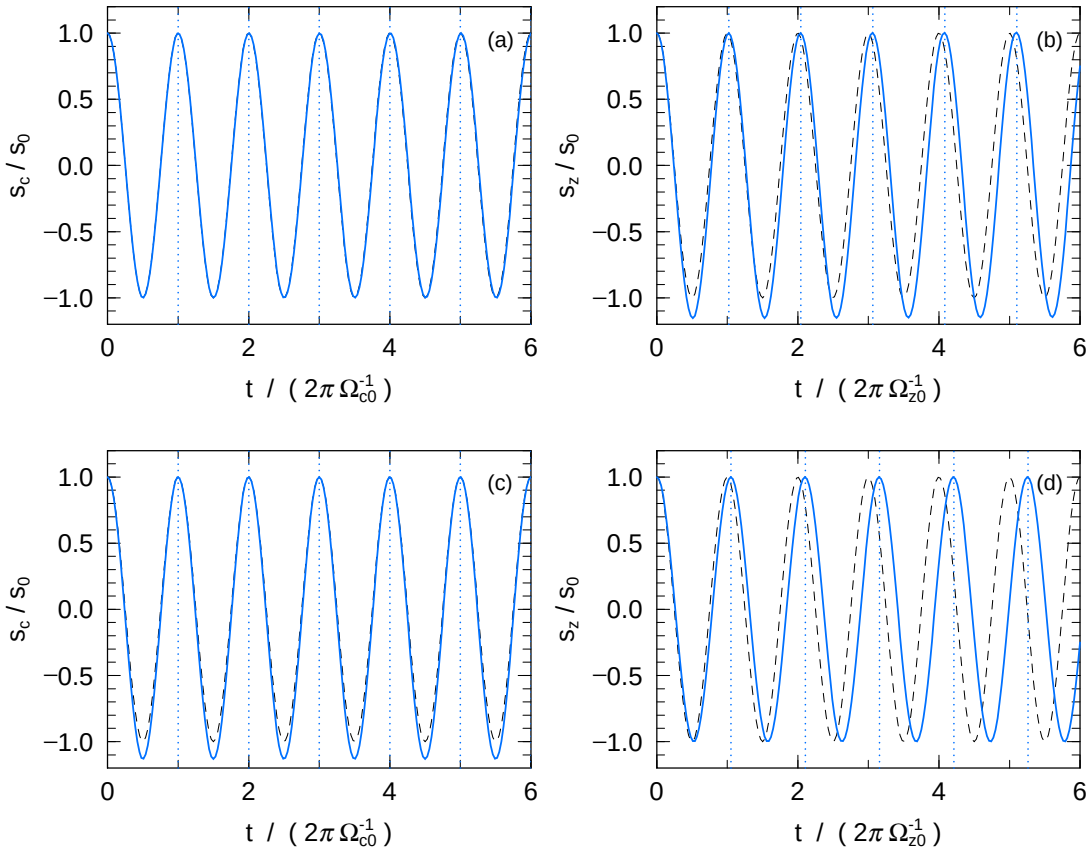

FIG. 8: (color online) The time evolution of the collective coordinates s_c [(a) (c)] and s_z [(b) (d)] in the oblate deformed potential ($\omega_z/\omega_c = 80$) when $N = 10^4$ [(a) (b)] and in the prolate deformed potential ($\omega_c/\omega_z = 600$) when $N = 10^3$ [(c) (d)]. The short-dashed lines represent the results when $g = 0$; the solid lines and the dotted separations represent the results and the periods of the normal modes when $g = 0.3\omega_c^{-1/2}$ [(a) (b)] or $0.2\omega_z^{-1/2}$ [(c) (d)], respectively.

Eqs. (85) and (86); when the λ_z in Eq. (85) (λ_c in Eq. (86)) is nearly constant in time as the slower oscillations, the mixing term $\gamma_c\lambda_z$ in Eq. (85) ($\gamma_z\lambda_c$ in Eq. (86)) gives the center shift.

Here it should be noted that the mixing does not affect the frequency of the normal modes in the first order terms, so that the mixing effects principally appear in the center shifts of the faster oscillations; furthermore we can say that the faster oscillations can exhibit well collectivity at the anisotropic limits because the atoms there take same one-particle energy-level in the narrower direction motions, and the one-particle wave-functions only within the energy-level principally determine the behaviors of the faster oscillations just like as the

collective oscillations of the BECs, where the strength functions take nearly a single peak in the excited energy. Thus we point out that the faster oscillations must include the detailed informations of the super-anisotropic deformed gases.

V. SUMMARY AND OUTLOOK

In the present work, we study the breathing oscillations of the fermion condensates in the anisotropic harmonic oscillator traps. If anisotropy of the traps is not so large, the gases behave as the 3D gases; otherwise the gases exhibit the QLD properties owing to the QLD shell-structures associated with the trap anisotropy. We theoretically reveal the effects of the QLD shell-structures on the breathing oscillations of the week-interacting fermion condensates with same number densities and describe the crossover behaviors between the 3D and QLD gases by developing TFA to the super-anisotropic systems.

The collective frequencies of the breathing oscillations are calculated in the scaling and sum-rule methods with the parameters determined in the perturbation theory and ETFA up to the first order of the inter-atomic interaction. As a result, it turned out that the effects of the QLD shell-structures disappear in the frequency of the transverse normal mode and appear only in that of the longitudinal normal mode with the hierarchic structures associated with the trap anisotropy. The results in ETFA with the finite cut-off energy theoretically reproduce the hierarchic structures below the cut-off energy, and agree with the exact results for the proper cut-off energy.

Finally we also demonstrate the time-evolution of the breathing oscillations in the present framework. In conclusion, we clarify the two kinds of influence of the inter-atomic interaction on the transverse and longitudinal oscillations: the frequency decrements (increments) in the longitudinal oscillations when $g > 0$ (< 0) and the center shifts in the faster oscillations.

The results in the present work give a theoretical prediction for the precise observations in the weekly interacting gases. If the inter-atomic interaction is very strong, our method is not applicable, and the oscillation properties may be different from our results. In addition, when the oscillations are including more than one strong oscillation modes, e.g. near the phase-separation or collapse, the scaling and sum-rule methods in this work should not be applied. In those cases, one should do more detailed investigation in the full-microscopic RPA or other direct time-evolution approaches compatible with the super-anisotropic systems [32, 33].

Asymmetric two-component gases in the super-anisotropic traps are another interesting topic. In that case, the breathing oscillations implicitly include not only the in-phase oscillations but also the out-of-phase oscillations, and exhibit coupled oscillations of the in-phase and out-of-phase oscillations [1]. We should study the ground state properties and collective excitations in another paper.

Acknowledgments

The authors would like to thank Prof. Toru Suzuki for useful discussions.

APPENDIX A: SCALING AND SUM-RULE METHODS

The scaling method gives the density matrix in the collective oscillation by an excitation operator $\mathcal{O}$:

$$\varrho(\lambda, \dot{\lambda}) = U(\lambda, \dot{\lambda}) \varrho_0 U^\dagger(\lambda, \dot{\lambda}) \tag{A1}$$

with a unitary operator

$$U(\lambda, \dot{\lambda}) = e^{i\dot{\lambda}\mathcal{O}} e^{\lambda[H,\mathcal{O}]}, \tag{A2}$$

where λ is the scaling amplitude of the collective oscillation and $\dot{\lambda}$ indicates the time derivative. Here the density matrices are normalized, $\mathrm{tr}\,(\varrho) = \mathrm{tr}\,(\varrho_0) = 1$, and the expectation values of an arbitrary operator A are given by $\langle A \rangle = \mathrm{tr}\,(\varrho A)$ and $\langle A \rangle_0 = \mathrm{tr}\,(\varrho_0 A)$.

The time-dependent variational principle,

$$\delta \int dt \left\langle i\frac{d}{dt} - H \right\rangle \equiv \delta \int dt\ \mathcal{L}[\lambda, \dot{\lambda}] = 0, \tag{A3}$$

gives the Euler-Lagrange equation for the generalized dynamical variable λ. By substituting Eq. (A1) into Eq. (A3), we can write the Lagrangian $\mathcal{L}$ in Eq. (A3) as

$$\mathcal{L}[\lambda, \dot{\lambda}] \simeq \left\langle [[\mathcal{O}, H], \mathcal{O}] \right\rangle_0 \dot{\lambda}^2 - \frac{1}{2} \left\langle [[\mathcal{O}, H], [H, [H, \mathcal{O}]]] \right\rangle_0 \lambda^2 \tag{A4}$$

to the second order in λ beside the constant term of λ.

When the density matrices are pure states, i.e. $\varrho_0 = \left|\Psi_0\right\rangle\left\langle\Psi_0\right|$, the coefficients in Eq. (A4) becomes

$$\left\langle [[\mathcal{O}, H], \mathcal{O}] \right\rangle_0 = M_1, \quad \frac{1}{2} \left\langle [[\mathcal{O}, H], [H, [H, \mathcal{O}]]] \right\rangle_0 = M_3 \tag{A5}$$

with the n-th moment

$$M_n \equiv \sum_{\nu\neq 0}(E_\nu - E_0)^n \left|\left\langle \Psi_\nu \middle| \mathcal{O} \middle| \Psi_0 \right\rangle\right|^2, \tag{A6}$$

where $\left|\Psi_\nu\right\rangle$ is the ν-th state with the energy E_ν in a complete set. As a result, the frequency of the collective oscillation can be written as

$$\Omega = \sqrt{\frac{M_3}{M_1}}. \tag{A7}$$

This result is equivalent to that in the sum-rule method.

APPENDIX B: THOMAS-FERMI APPROXIMATION

In the one-particle picture, the Wigner function in Eq. (45) can be described as

$$f(\boldsymbol{r},\boldsymbol{p}) = \int d\varepsilon\ F(\varepsilon)D(\varepsilon)f^{(\mathrm{op})}(\boldsymbol{r},\boldsymbol{p};\varepsilon), \tag{B1}$$

where we use the Fermi distribution function $F(\varepsilon) \equiv 1/(\exp(\beta(\varepsilon-\mu_{\mathrm{F}}))+1)$ and introduce the one-particle Wigner function

$$f^{(\mathrm{op})}(\boldsymbol{r},\boldsymbol{p};\varepsilon) \equiv \sum_n \delta_{\varepsilon,\epsilon_n} \int d\boldsymbol{s}\ e^{-i\boldsymbol{p}\cdot\boldsymbol{s}} \phi_n^*\left(\boldsymbol{r}-\frac{\boldsymbol{s}}{2}\right)\phi_n\left(\boldsymbol{r}+\frac{\boldsymbol{s}}{2}\right) \tag{B2}$$

and energy-level density

$$D(\varepsilon) \equiv \sum_n \delta(\varepsilon-\epsilon_n) \tag{B3}$$

with one-particle energy ϵ_n.

In TFA, the Wigner function in Eq. (B1) is evaluated with a semi-classical way:

$$D(\varepsilon)f^{(\mathrm{op})}(\boldsymbol{r},\boldsymbol{p};\varepsilon) \approx \delta\left(\varepsilon - e_{\mathrm{cl}}(\boldsymbol{r},\boldsymbol{p})\right) \tag{B4}$$

or

$$f(\boldsymbol{r},\boldsymbol{p}) \approx F(e_{\mathrm{cl}}(\boldsymbol{r},\boldsymbol{p})) \tag{B5}$$

with the classical energy $e_{\mathrm{cl}}(\boldsymbol{r},\boldsymbol{p})$, where we keep the quantum statistics, $F(\varepsilon)$, and approximate the quantum motion and energy-level density into these of the classical mechanics. This result is also obtained by the semi-classical $\hbar$ expansion [34].

The classical energy-level density can be obtained by integrating Eq. (B4) in the phase-space owing to the normalization of the one-particle Wigner function: e.g. in the d-dimensional harmonic oscillator potentials ($d = 1, 2, \dots$),

$$e_{\mathrm{cl}}(\boldsymbol{r},\boldsymbol{p}) = \frac{p^2}{2} + \frac{1}{2}\sum_{j=1}^{d}\omega_j^2 r_j^2, \tag{B6}$$

the classical energy level densities $D^{(d)}(\varepsilon)$ become

$$D^{(d)}(\varepsilon) = \frac{\varepsilon^{d-1}}{(d-1)!} \left(\prod_{j=1}^{d} \omega_j \right)^{-1} \Theta(\varepsilon) \tag{B7}$$

with the Heaviside's step function $\Theta(x)$.

---

[1] T. Maruyama and T. Nishimura, Phys. Rev. A **75**, 033611 (2007).

[2] For reviews, see A. S. Parkins and H. D. F. Walls, Phys. Rep. **303**, 1 (1998); F. Dalfovo, S. Giorgini, L. P. Pitaevskii, and S. Stringari, Rev. Mod. Phys. **71**, 463 (1999); W. Ketterle, D. S. Durfee, and D. M. Stamper-Kum, in *Bose-Einstein Condensation in Atomic Gases*, Proceedings of International School of Physics "Enrico Fermi", edited by M. Ingusico, S. Stringari and C. Wieman (IOS Press, Amsterdam, 1999); C. J. Pethik and H. Smith, *Bose-Einstein Condensation in Dilute Gases* (Cambridge University Press, Cambridge, 2002).

[3] E. A. Cornell and C. E. Wieman, Rev. Mod. Phys. **74**, 875 (2002); W. Ketterle, Rev. Mod. Phys. **74**, 1131 (2002).

[4] M. H. Anderson, J. R. Ensher, M. R. Matthews, C. E. Wieman, and E. A. Cornell, Science **269**, 198 (1995); K. B. Davis, M. O. Mewes, M. R. Andrews, N. J. van Druten, D. S. Durfee, D. M. Kurn, and W. Ketterle, Phys. Rev. Lett. **75**, 3969 (1995).

[5] B. DeMarco and D. S. Jin, Science **285**, 1703 (1999).

[6] S. R. Granade, M. E. Gehm, K. M. O'Hara, and J. E. Thomas, Phys. Rev. Lett. **88**, 120405 (2002).

[7] A. G. Tuscott, K. E. Strecker, W. I. McAlexander, G. B. Parridge, and R. G. Hullet, Science **291**, 2570 (2001).

[8] F. Schreck, L. Khaykovich, K. L. Corwin, G. Ferrari, T. Bourdel, J. Cubizolles, and C. Salomon, Phys. Rev. Lett. **87**, 080403 (2001).

[9] Z. Hadzibabic, C. A. Stan, K. Dieckmann, S. Gupta, M. W. Zwierlein, A. Gorlitz, and W. Ketterle, Phys. Rev. Lett. **88**, 160401 (2002).

[10] Z. Hadzibabic, S. Gupta, C. A. Stan, C. H. Schunck, M. W. Zwierlein, K. Dieckmann, and W. Ketterle, Phys. Rev. Lett. **91**, 160401 (2003).

[11] C. A. Regal, M. Greiner, and D. S. Jin, Phys. Rev. Lett. **92**, 040403 (2004); M. Bartenstein, A. Altmeyer, S. Riedl, et.al., Phys. Rev. Lett. **92**, 120401 (2004); M. N. Zwierlein, C. A. Stan,

C. H. Schunck, et.al., Phys. Rev. Lett. **92**, 120403 (2004).

[12] For reviews, see S. Giorgini, L. P. Pitaevskii, and S. Stringari, Rev. Mod. Phys. 80, 1215 (2008).

[13] T. Sogo and H. Yabu, Phys. Rev. A **66**, 043611 (2002).

[14] A. Görlitz, J. M. Vogels, A. E. Leanhardt et.al., Phys. Rev. Lett. **87**, 130402 (2001).

[15] S. Dettmer, D. Hellweg, P. Ryytty et.al., Phys. Rev. Lett. **87**, 160406 (2001).

[16] F. Schreck, L. Khaykovich, K. L. Corwin, G. Ferrari, T. Bourdel, J. Cubizolles, and C. Salomon, Phys. Rev. Lett. **87**, 080403 (2001).

[17] T. Stöferle, H. Moritz, C. Schori, M. Kohl, and T. Esslinger, Phys. Rev. Lett. **92**, 130403 (2004).

[18] H. Ott, J. Fortagh, G. Schlotterbeck, A. Grossmann, and C. Zimmermann, Phys. Rev. Lett. **87**, 230401 (2001).

[19] W. Hänsel, P. Hommelhoff, T. W. Hänsch, J. Reichel, Nature **413**, 498 (2001).

[20] J. H. Thywissen, M. Olshanii, G. Zabow et.al., Eur. Phys. J. D **7**, 361 (1999).

[21] S. Schneider, A. Kasper, Ch. vom Hagen et.al., Phys. Rev. A **67**, 023612 (2003).

[22] For review, see L. Pitaevskii and S. Stringari, *Bose-Einstein Condensation* (Clarendon Press, Oxford, 2003); D. S. Petrov, D. M. Gangardt, and G. V. Shlyapnikov, J. Phys. IV **116**, 3 (2006).

[23] G. M. Bruun, Phys. Rev. A **63**, 043408 (2001).

[24] K. Goral, M. Brewczyk, and K. Rzazewski, Phys. Rev. A **67**, 025601 (2003).

[25] G. M. Bruun and B. R. Mottelson, Phys. Rev. Lett **87**, 270403 (2001).

[26] L. Vichi and S. Stringari, Phys. Rev. A **60**, 4734 (1999).

[27] G. F. Bertsch, Nucl. Phys. A **249**, 253 (1975); G. F. Bertsch and K. Stricker, Phys. Rev. C **13**, 1312 (1976); D. M. Brink and R. Leobardi, Nucl. Phys. A **258**, 285 (1976); T. Suzuki, Prog. Theor. Phys. **64**, 1627 (1980).

[28] O. Bohigas, A. M. Lane, and J. Martorell, Phys. Rep. **51**, 267 (1979).

[29] T. Maruyama and G. F. Bertsch, Phys. Rev. A **73**, 013610 (2006).

[30] A. L. Fetter and J. D. Walecka, *Quantum theory of many-particle systems* (McGrawHill, NY, 1971).

[31] The precise structures of the one-particle energy-level densities are well-studied in the Nilsson model for nuclear physics; See P. Ring and P. Schuck, *The Nuclear Many-Body Problem*

(Springer, New York, 2000).

[32] T. Maruyama, H. Yabu, and T. Suzuki, Phys. Rev. A **72**, 013609 (2005).

[33] T. Maruyama and G. F. Bertsch, Phys. Rev. A **77**, 063611 (2008).

[34] R. G. Parr and W. Yang Weitao, *Density-functional Theory of Atoms And Molecules* (Oxford University Press, NewYork, 1989).

[35] If we consider the quantum number of the coarse mode as a component number, the 3D gas can be considered as a multi-component mixture of the QLD gases. Thus the dimensionality is related to the multiplicity.

[36] The $\lambda_{c,z}(t)$ are taken as the c-numbers in the scaling method, so that the classical system in Eqs. (22) and (30) must contain the quantum fluctuations as mean-values. This property originally comes from the time-dependent HF theory.

[37] The coarse graining is due to the multi-time-scale structures derived from the QLD shell-structures, and yields the QLD properties in the slowest time-scale with renormalization of the freedom degrees associated with the other time-scales as plotted in Fig. 8.